Proc. Natl. Acad. Sci. USA
Vol. 96, pp. 7928–7931, July 1999
Cell Biology

Arrangement of radial actin bundles in the growth cone of *Aplysia* bag cell neurons shows the immediate past history of filopodial behavior

(nerve cell growth/cell motility/actin filaments/polarized light microscopy)

KAORU KATOH, KATHERINE HAMMAR, PETER J. S. SMITH, AND RUDOLF OLDENBOURG*

Marine Biological Laboratory, Woods Hole, MA 02543

Communicated by Shinya Inoue, Marine Biological Laboratory, Woods Hole, MA, May 17, 1999 (received for review January 1, 1999)

ABSTRACT **Filopodia that protrude forward from the lamellipodium, located at the leading edge of a neuronal growth cone, are needed to guide the extension of a nerve cell. At the core of each filopodium an actin bundle forms and grows into the lamellipodium. By using kymographs of time-lapse polarized light images we examined the relationship between the behavior of the filopodia, the actin bundles immediately proximal to the filopodia, and the shapes and composition of actin bundles in the whole lamellipodium. We find that the shapes of actin bundles, such as tilt, fork, and fused zones, originate at the leading edge and are surprisingly well preserved during retrograde transport of the actin cytoskeleton in the whole lamellipodium. The number of filaments that make up the radial actin bundles, as displayed by their birefringence retardation, also is preserved during retrograde flow over a distance of 4–8 μm from the leading edge into the lamellipodium. Thus, the disposition of the actin bundles in the lamellipodium frozen at any time point preserves and portrays a history of the past behavior of actin bundles proximal to the filopodia and the behavior of the filopodia themselves. These findings suggest that the arrangement of actin bundles in static image records, such as electron or fluorescence micrographs of fixed and stained specimens, can in fact reveal the sequence of the past history of filopodial behavior and the generation, density, fusion, etc. of the filaments in the actin bundles.**

The outgrowth of a nerve cell is guided by a growth cone at the leading tip of the cell (1–4). As in many other motile cells, the growth cone of a neurite typically has a wide and thin lamellipodium with radially aligned, finger-like filopodia that protrude at the leading edge (Fig. 1*A*). The motility of the growth cone is believed to depend on the cytoskeleton of the lamellipodium that is rich in filamentous actin but poor in microtubules (5–15). At least two types of actin-based structures can be distinguished in the lamellipodium: the radially aligned actin bundles and the space-filling network of actin filaments (16).

One of the best-known aspects of actin dynamics in lamellipodia is retrograde flow of filamentous actin. In retrograde flow, the actin network and radial bundles are transported from the leading edge of the growth cone to its central domain (7, 14, 15, 17–20). Retrograde flow of filamentous actin (f-actin) in lamellipodia previously was confirmed by using fluorescently labeled or unlabeled cells (7, 21, 22). Myosin molecules presumably are involved in powering retrograde flow (23, 24). Retrograde flow occurs simultaneously with actin polymerization near the leading edge and its depolymerization near the central domain. Thus, the actin-based cytoskeleton in the lamellipodium maintains a dynamic equilibrium between actin assembly near the leading edge, retrograde flow, and disassembly of actin filaments near the central domain.

Another important aspect of f-actin dynamics is the behavior of radial actin bundles associated with filopodia as revealed by recent light microscopic studies (15, 20, 25). These studies demonstrated that radial actin bundles in the lamellipodium show complicated behaviors, including generation, lateral movement, and fusion with adjacent actin bundles. These motile events appear to be linked to similar behaviors of filopodia that occur at the leading edge.

We have observed the cytoskeletal dynamics in growth cones of *Aplysia* bag cell neurons by using a new type of polarized light microscope (26, 27). The Pol-Scope provides fast time-lapse measurements of birefringent fine structure at high image resolution that can be directly and quantitatively interpreted in terms of submicroscopic molecular order such as the number of filaments in a bundle (Fig. 1).

Pol-Scope images reveal important structural elements of the growth cone without having to treat the cells with exogenous dyes or fluorescent labels. Time-lapse movies of Pol-Scope images vividly display the architectural dynamics of filopodia and actin bundles that can be observed continuously for long time periods (15 min and more) without degrading image contrast or adversely affecting the cell. These characteristics provide distinct advantages compared with fluorescence and differential interference contrast microscopy and provide insights into the dynamic architecture of motile cells. A general description of our observations of growth cones of *Aplysia* bag cell neurons by using the Pol-Scope was published recently, together with time-lapse movies of the birefringent fine structure in the lamellipodium (25).

In this paper we describe our analysis of the relationship between the behavior of the filopodia, the actin bundles located near the leading edge, and the shape of actin bundles in the whole lamellipodium. We analyzed movie records by constructing images, so-called kymographs, from image strips copied from regions near the leading edge. As discussed in this paper, the kymographs, which show the behavior of the proximal actin bundles, represent, in two-dimensional layouts, the recent history of filopodial behavior, including their creation, lateral travel, and fusion with neighboring filopodia. These "synthetic" kymographs look strikingly similar to the arrangement of actin bundles in the whole lamellipodium observed at a single time point at the termination of the kymograph. Therefore, we conclude that the arrangement and composition of actin bundles in the whole lamellipodium at any given instant is itself a natural kymograph holding a record of the most recent history of filopodial behavior.

MATERIALS AND METHODS

Cell Culture. Primary cell cultures of *Aplysia* bag cell neurons (28, 29) were cultured on a coverslip bathed in

*To whom reprint requests should be addressed at: Marine Biological Laboratory, 7 MBL Street, Woods Hole, MA 02543-1015. e-mail: rudolfo@mbl.edu.

PNAS is available online at www.pnas.org.

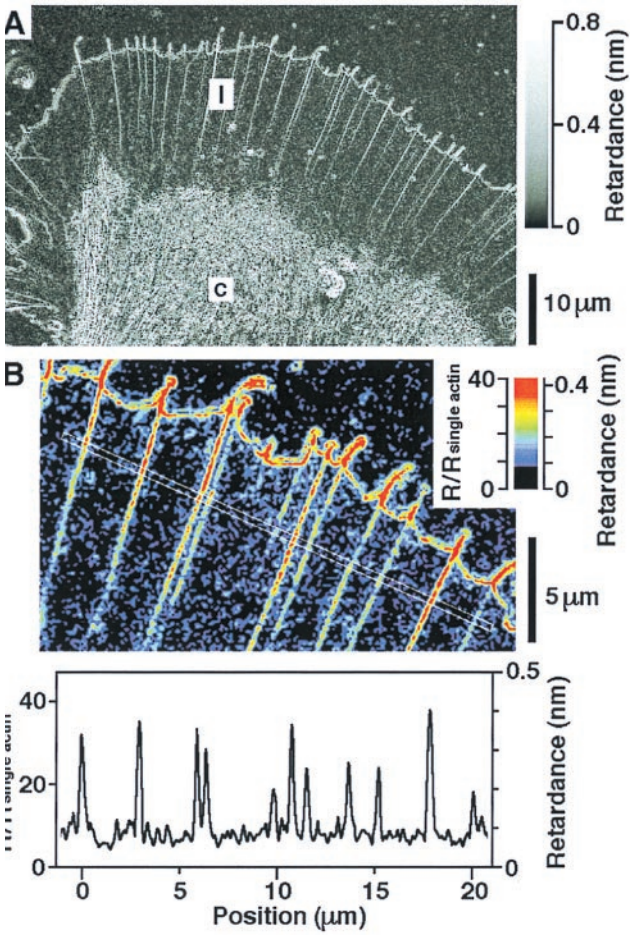

FIG. 1. Birefringent fine structure of the living *Aplysia* bag cell growth cone recorded with the Pol-Scope. (*A*) Retardance map of a growth cone. The leading edge (top) shows many finger-like protrusions, or filopodia. Behind the leading edge in the peripheral lamellar domain (or lamellipodium, l), birefringent fibers (bundles of actin filaments) are aligned radially. The central domain (c) is filled with vesicles and highly birefringent fibers (microtubules). Gray scale: Retardance in nm. (*B*) Birefringence of actin bundles measured as retardance and shown in pseudo color and as a profile plot. The pseudo color map shows the enlarged middle portion of the peripheral lamellar domain in *A*. The profile plot shows retardances measured in the white box in the map. Sharp peaks represent actin bundles. Maximum peak values are the retardances of the bundles. R/R_{single} is the retardance divided by that of a single actin filament, which estimates the number of actin filaments within a bundle (see *Materials and Methods*).

artificial seawater. Growth cones were observed after 1 or 2 days from starting the primary cell culture. For observation, the coverslips were mounted on glass slides with thin spacers (150 μm) and sealed to prevent evaporation. All observations were made at room temperature and within 4 hr of sealing the preparation.

Birefringence Imaging and the Pol-Scope. To directly observe actin bundles in living unstained growth cones noninvasively, we measured and displayed the optical anisotropy (birefringence) of the cellular fine structures (30, 31). Birefringence is an optical property that is a consequence of molecular order in the sample. For example, long, thin filaments such as those that make up the actin bundles are birefringent.

To visualize the dynamics of actin bundles in the living growth cone, we imaged their birefringence and made time-lapse movies by using the Pol-Scope. The Pol-Scope achieves high sensitivity and high resolution by enhancing the traditional polarizing microscope with electro-optical devices, electronic imaging, and digital image analysis (26, 27, 31). The Pol-Scope provides images whose brightness for each pixel is strictly proportional to the birefringence retardation of the particular object point and independent of its slow axis orientation. Thus, unlike conventional polarizing microscopes, it provides a calculated birefringence distribution map that has no blind direction regardless of the orientation of molecular or fine-structural axis in the image plane. The slow axis orientation of the object points also can be displayed on an azimuth map.

The Pol-Scope measures birefringence as birefringence retardation, which is also called retardance. When light passes through a birefringent sample, the light wave is separated into two orthogonally polarized waves (o-ray and e-ray). The two waves travel at different speeds and, therefore, leave the sample with a different phase. The phase shift between the light waves is called retardance and is measured as a length in nm (32). In the Pol-Scope images, measured retardances are represented as gray values or pseudo colors (see e.g., Fig. 1).

The microscope setup used to record raw image data is described in more detail in ref. 25. As imaging lenses we used an oil immersion $\times 60/1.4$ numerical aperture plan apochromat objective lens and matching condenser lens with aperture diaphragm set to 1.0 NA (Nikon).

Estimating the Number of Filaments in Actin Bundles. The retardance of a filament bundle can be interpreted in terms of the number of filaments in the bundle (33, 34). When the diameter of the bundle is only a fraction of the wavelength of light, the retardance (R) of the bundle is directly proportional to the number (N) of filaments: $R = N \cdot R_{single}$, where R_{single} is the retardance of a single filament in the bundle. Based on measurements of the acrosomal process of horseshoe crab sperms, we estimated the retardance of a single actin filament, including actin-associated proteins, to be $R_{single} = 0.0107$ nm (35). Figures in this paper show $N = R/R_{single}$ of actin bundles in pseudo color images or in profile plots. As shown in the profile plot of Fig. 1*B*, the number of actin filaments per bundle ranges between 18 and 40 filaments, a range that is similar to results reported from an electron microscopy study of vertebrate neurons (16).

Looking at the pseudo color image and profile plot of Fig. 1*B*, the question arises how to account for the background retardance when measuring the peak bundle value for estimating the number of filaments in a bundle. To arrive at the correct bundle retardance, one might expect it to be necessary to subtract from the peak value the average background retardance of approximately 0.08 nm that shows up in locations between bundles. However, the small birefringent specs making up the background in the pseudo color image have slow axis directions that change randomly, as displayed in the concurrently measured azimuth map (not shown). Hence, the background that superimposes on the bundle can either add or subtract from the bundle retardance. Therefore, the background retardance does not alter the average bundle retardance.

RESULTS AND DISCUSSION

In a simple model of actin turnover, actin bundles are assembled at their barbed end near the leading edge and then moved rearward to the central region of the growth cone by retrograde transport (Fig. 2*A*). This model of continuous assembly and rearward motion of actin bundles places the bundle segments in strict chronological order. Segments near the leading edge were assembled last, whereas segments further away from the edge were assembled earlier.

Guided by this model, we constructed kymographs from thin image strips that recorded the position and size of actin bundles near the leading edge. The strips were made into

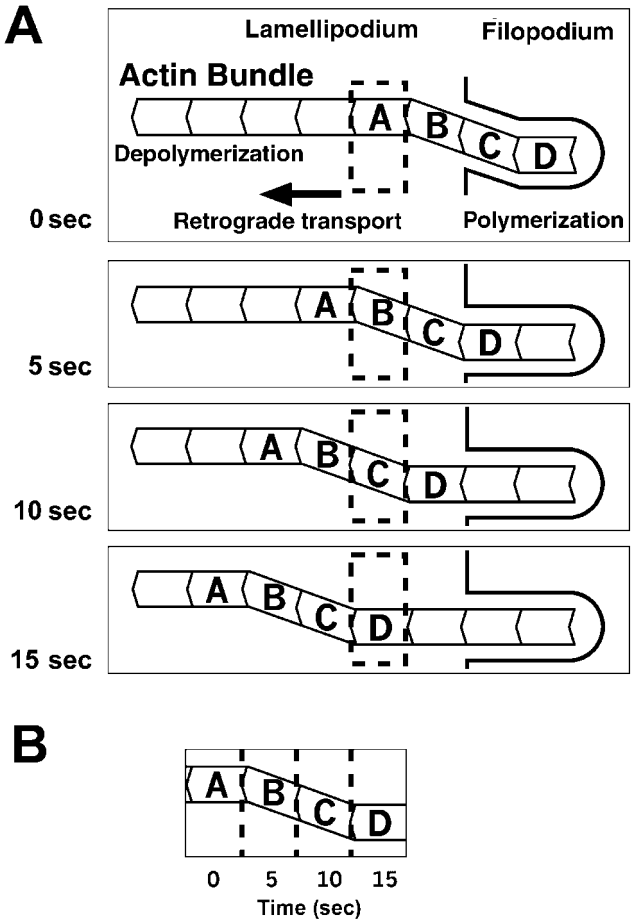

FIG. 2. Proposed schematic of retrograde flow of actin bundle and kymographic analysis. (*A*) A chronological series of schematic snapshots showing a radial actin bundle inside a filopodium and the lamellipodium. Retrograde flow in the lamellipodium moves the actin bundle out of the filopodium in which actin units are continuously added to the bundle end. A kink in the actin bundle (segments A, B, C, D) is maintained during retrograde transport. (*B*) A kymograph assembled from image portions indicated by dashed frames in *A*. The image portions were arranged in chronological order along the horizontal direction. The actin bundle in the kymograph should be similar in appearance to the bundle shown in the last frame (15 sec) in *A*, if the bundle does not significantly change its shape or assembly state during retrograde flow.

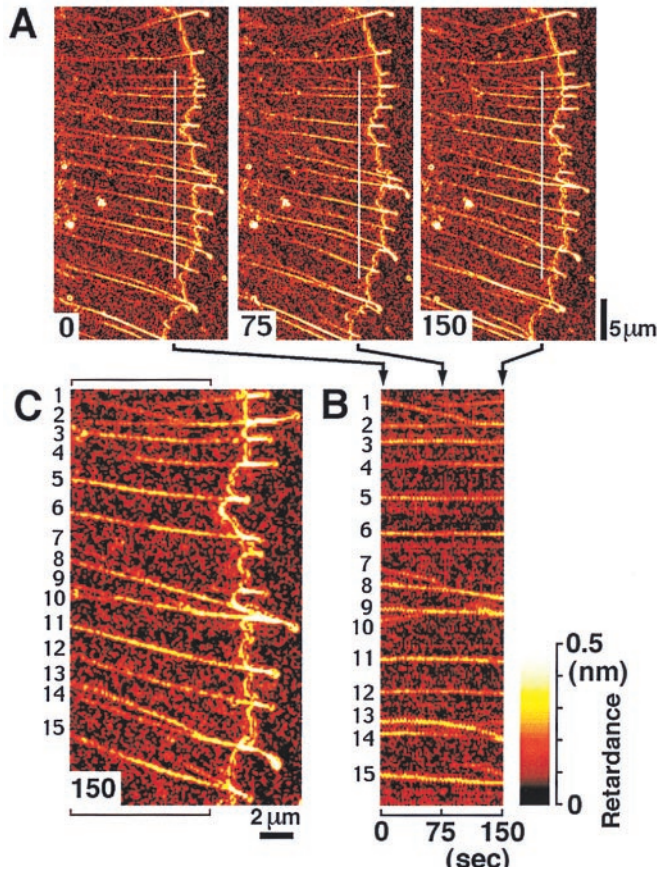

FIG. 3. Dynamics of actin bundle arrangement in the lamellipodium of a growth cone and assembly of a kymograph. (*A*) Individual retardance maps from a time-lapse movie of a wide growth cone. Numbers at bottom left of images show time in sec. The white lines indicate the long, narrow image strips near the leading edge that were used in assembling the kymograph in *B*. The strips had a width of 0.25 μm, which corresponds to the average distance traveled by retrograde flow between two consecutive movie frames (5-sec interval). (*B*) Kymograph assembled from image strips taken from 31 consecutive retardance maps. In the kymograph, the image strips are placed chronologically from 0 sec to 150 sec, in 5-sec intervals. Numbers on the left near the vertical image border identify corresponding actin bundles in *C*. (*C*) Magnified tip region of the lamellipodium at time 150 sec in *A*. The brackets on top and bottom indicate the approximate dimensions of *B*. Except for the convergence of the actin bundles toward the central domain of the lamellipodium (left side of *C*), the actin bundle arrangement in the kymograph in *B* is strikingly similar to those in the lamellipodium.

kymographs by placing them next to each other in chronological order (Fig. 2*B*). The placement of bundle segments in a kymograph is expected to reflect the state and location of bundle segments in the lamellipodium. Thus, we hypothesize that the shape and composition of actin bundles in a kymograph should be similar to that in the whole lamellipodium viewed at the termination of the kymograph, if the bundles do not significantly change their shapes, relative speed, lateral positions, or assembly states during retrograde flow.

Fig. 3 *A* and *C* shows a wide lamellipodium from which a kymograph containing some 15 actin bundles was assembled (Fig. 3*B*). The shapes of the actin bundles in the kymograph are remarkably similar to those in the lamellipodium of Fig. 3*C* (an enlargement of the tip region at time 150 sec in Fig. 3*A*). Apparently, the radial actin bundles in the lamellipodium are in fact arranged quite similarly to those in the kymograph. This similarity supports our hypothesis shown in Fig. 2 and stated at the end of the previous paragraph and suggests that the shape and composition of actin bundles in the lamellipodium directly reflect the movement and other changes of the filament bundles that took place near their tips (located in the filopodia). In other words, the arrangement and composition of actin bundles are determined near the leading edge and are not significantly changed during retrograde flow.

The findings reported here are based on the recording and careful analysis of more than 100 time-lapse movies. A time-lapse record typically lasted over 15–30 min, with data recorded at time intervals of 5–30 sec. For the study reported here, several time-lapse movies, which were recorded by using different growth cones, were analyzed by using the kymographic method. The figures shown in this paper present typical results, and our conclusions are based on the analysis of all of our experimental observations.

Actin bundles in lamellipodia typically are associated with filopodia. The base of a filopodium is located at the leading edge and is not far from the image strip used for making a kymograph. Therefore, the position of an actin bundle in an image strip should closely reflect the position of the base of the associated filopodium. Furthermore, we find that movements of the filopodium lead to changes in the position, tilt, fusion,

etc. of the filopodium as well as of the associated actin bundle (25). Thus, kymographs of the proximal actin bundles reflect the history of the immediate past movements and behavior of filopodia.

Just like a kymograph reflects the history of past filopodial behavior, so does the arrangement of actin bundles in the whole lamellipodium. Actin bundles in lamellipodia show characteristic shapes such as tilts, forks, and fused zones (Fig. 3*A*). Based on our observations, we find that these shapes are related to specific behaviors of filopodia. For example, a laterally traveling filopodium created a tilted actin bundle in the lamellipodium. When the traveling filopodium merged with a neighboring filopodium, the two associated bundles created a fork followed by a fused zone with increased retardance. In each case, the characteristic shape was created near the leading edge and then transported into the lamellipodium by retrograde flow.

Notwithstanding the striking similarities, there are some systematic differences in the arrangement and composition of actin bundles in the kymographs and lamellipodia. For example, the procedure of assembling a kymograph produces a rectangular layout of the fiber arrangement. The growth cone, however, shows a more radial arrangement of the fibers, seemingly compressing regions close to the central domain. The composition of actin bundles also shows some change during retrograde flow. Starting from the leading edge, bundle segments usually maintain their birefringence retardation over several microns into the lamellipodium. Abrupt changes in bundle composition caused by the merging of two bundles, for example, is propagated into the lamellipodium at the speed of retrograde flow and remains unchanged over distances of 4–8 μm (see figure 6 in ref. 25). At larger distances from the leading edge, however, the retardance of a bundle in the lamellipodium decreases, suggesting that at sufficiently large distances from the leading edge bundle segments start to lose filaments. Changes that occur behind the image strip proximal to the leading edge obviously are not reflected in a kymograph. The analysis of the differences in the arrangement and composition of actin bundles in kymographs and lamellipodia therefore can lead to further insights into the architectural dynamics of the cytoskeleton. These include the mapping of speed and direction of the retrograde flow field in the lamellipodium and an analysis of actin depolymerization that occurs near the central domain.

In conclusion, we show that the arrangement of actin bundles in the lamellipodium of the neuronal growth cone is akin to a ''living'' kymograph recording at any instant in time the recent history of f-actin and filopodial movement and behavior near the leading edge. This finding opens up the possibility of interpreting the arrangement of actin bundles in static image records, such as electron or fluorescence micrographs of fixed and stained specimens, to reveal the recent dynamic history of actin filament and filopodial behavior.

We are grateful to Shinya Inoué of the Marine Biological Laboratory for his invaluable suggestions and encouragement during the course of this work and his critical reading of the manuscript. We acknowledge support from the BioCurrent Research Center, supported by National Institutes of Health Grant P41RR01395. This work was funded by National Institutes of Health Grant GM 49210 awarded to R.O.

1. Cajal, S. R. y. (1909) *Histologie du système nerveux de l'homme et des vertébrés* (Maloine, Paris), Vol. 1.
2. Cajal, S. R. y. (1911) *Histologie du système nerveux de l'homme et des vertébrés* (Maloine, Paris), Vol. 2.
3. Cajal, S. R. y. (1995) *Histology of the Nervous System of Man and Vertebrates* (Oxford Univ. Press, New York), Vols. 1 and 2.
4. Letourneau, P. C., Kater, S. B. & Macagno, E. R., eds. (1991) *The Nerve Growth Cone* (Raven, New York).
5. Yamada, K. M., Spooner, B. S. & Wessells, N. K. (1971) *J. Cell Biol.* **49,** 614–635.
6. Tosney, K. W. & Wessells, N. K. (1983) *J. Cell Sci.* **61,** 389–411.
7. Forscher, P. & Smith, S. J. (1988) *J. Cell Biol.* **107,** 1505–1516.
8. Bridgman, P. C. & Dailey, M. E. (1989) *J. Cell Biol.* **108,** 95–109.
9. Lin, C. H. & Forscher, P. (1993) *J. Cell Biol.* **121,** 1369–1383.
10. Lin, C.-H. & Forscher, P. (1995) *Neuron* **14,** 763–771.
11. Mitchison, T. J. & Cramer, L. P. (1996) *Cell* **84,** 371–379.
12. Theriot, J. A. & Mitchison, T. J. (1991) *Nature (London)* **352,** 126–131.
13. Thompson, C., Lin, C. H. & Forscher, P. (1996) *J. Cell Sci.* **109,** 2843–2854.
14. Welch, M. D., Mallavarapu, A., Rosenblatt, J. & Mitchison, T. J. (1997) *Curr. Opin. Cell Biol.* **9,** 54–61.
15. Welnhofer, E. A., Zhao, L. & Cohan, I. (1997) *Cell. Motil. Cytoskeleton* **37,** 54–71.
16. Lewis, A. K. & Bridgman, P. C. (1992) *J. Cell Biol.* **119,** 1219–1243.
17. Wang, Y. L. (1985) *J. Cell Biol.* **101,** 597–602.
18. Bray, D. & White, J. G. (1988) *Science* **239,** 883–888.
19. Smith, S. J. (1988) *Science* **242,** 708–715.
20. Izzard, C. S. (1988) *Cell Motil. Cytoskeleton* **10,** 137–142.
21. Okabe, S. & Hirokawa, N. (1991) *J. Neurosci.* **11,** 1918–1929.
22. Forscher, P., Lin, C. H. & Thompson, C. (1992) *Nature (London)* **357,** 515–518.
23. Wolenski, J. P., Cheney, R. E., Mooseker, M. S. & Forscher, P. (1995) *J. Cell Sci.* **108,** 1489–1496.
24. Lin, C. H., Espreafico, E. M., Mooseker, M. S. & Forscher, P. (1996) *Neuron* **16,** 769–782.
25. Katoh, K., Hammar, K., Smith, P. J. S. & Oldenbourg, R. (1999) *Mol. Biol. Cell* **10,** 197–210.
26. Oldenbourg, R. & Mei, G. (1995) *J. Microsc. (Oxford)* **180,** 140–147.
27. Oldenbourg, R. (1996) *Nature (London)* **381,** 811–812.
28. Knox, R. J., Quattrocki, E. A., Connor, J. A. & Kaczmarek, L. K. (1992) *Neuron* **8,** 883–889.
29. Kaczmarek, L. K., Finbow, M., Revel, J. P. & Strumwasser, F. (1979) *J. Neurobiol.* **10,** 535–550.
30. Inoué, S. (1986) *Video Microscopy* (Plenum, New York), 1st Ed., pp. 477–510.
31. Oldenbourg, R. (1999) in *Methods in Cell Biology: Mitosis and Meiosis*, ed. Rieder, C. (Academic, San Diego), Vol. 61, pp. 175–208.
32. Hecht, E. (1998) *Optics* (Addison–Wesley, Reading, MA).
33. Tran, P., Salmon, E. D. & Oldenbourg, R. (1995) *Biol. Bull.* **189,** 206.
34. Oldenbourg, R., Salmon, E. D. & Tran, P. T. (1998) *Biophys. J.* **74,** 645–654.
35. Katoh, K., Yamada, K., Oosawa, F. & Oldenbourg, R. (1996) *Biol. Bull.* **191,** 270–271.